crystalline phase.[2,17] Here, we demonstrate that copper sulphide NCs can be prepared through a single-source approach by thermolysis of Cu(II) dialkyldithiocarbamate complexes in ILs. Furthermore, the photocatalytic activity of the ensuing copper sulphide nanomaterials have been evaluated using rhodamine B (RhB) solutions under visible-light irradiation with the assistance of hydrogen peroxide.

Experimental

Reagents and methods

Copper nitrate tri-hydrate (Carlo Erba, 99.5%), dibutylamine (Sigma-Aldrich, 99%), carbon disulphide (Panreac), sodium hydroxide (Acros Organics, 98.5%), sodium diethyldithiocarbamate trihydrate (Sigma-Aldrich), oleylamine (Sigma-Aldrich) and 30% (w/w) aqueous hydrogen peroxide (Riedel-de-Häen) were used as received. The ionic liquids trihexyl(tetradecyl) phosphonium dicyanamide, [TDTHP][$N(CN)_2$] (Cytec, 96.5%), and trihexyl(tetradecyl) phosphonium bis(trifluoromethylsulfonyl)imide, [THTDP][NTf_2] (Cytec, 93.7%) were dried under moderate vacuum at room temperature, for a minimum of 72 h. All other solvents were supplied by commercial sources and used as received.

Copper diethyldithiocarbamate, {$Cu[S_2CN(C_2H_5)_2]_2$}, and copper dibutyldithiocarbamate, {$Cu[S_2CN(C_4H_9)_2]_2$}, were investigated as single-molecule precursors for copper sulphides and were prepared by adaptation of literature methods.[18,19] Hence, the compound {$Cu[S_2CN(C_2H_5)_2]_2$} was prepared by the addition of Cu(II) salt to a solution containing the diethyldithiocarbamate anion. In a typical procedure an aqueous solution of $Cu(NO_3)_2$ (10 mmol, 2.4 g) was treated, under stirring, with an excess of aqueous $Na(S_2CN(C_2H_5)_2)$. The brown solid obtained, {$Cu[S_2CN(C_2H_5)_2]_2$}, was collected by filtration and the final product recrystallized from hot acetone.[18]

{$Cu[S_2CN(C_2H_5)_2]_2$}. Microanalysis (wt%): found: C, 33.5; H, 4.98; N, 7.6; S, 35.4. Calc. for $Cu[S_2CN(C_2H_5)_2]_2$: C, 33.4; H, 5.6; N, 7.8; S, 35.6. ^{1}H NMR ($CDCl_3$) δ (ppm): 1.22 (t, 3H, CH_2CH_3); 3.73 (q, 2H, CH_2CH_3). {$Cu[S_2CN(C_4H_9)_2]_2$} was obtained by insertion of CS_2 into a secondary amine. Typically, butylamine (20 mmol) and then CS_2 (13.5 mmol) were added dropwise to 50 mL of $Cu(NO_3)_2$ (10 mmol) ethanolic solution at 60 °C. To this mixture, 20 mmol of NaOH have been added while stirring for 3 h at 60 °C. The brown solid formed was filtered and the product was recrystallized from hot acetone.[19]

{$Cu[S_2CN(C_4H_9)_2]_2$}. Microanalysis (wt%): found: C, 44.8; H, 6.9; N, 5.5; S, 28.0. Calc. for $Cu[S_2CN(C_4H_9)]_2$: C, 45.8; H, 7.7; N, 5.93; S, 27.1. ^{1}H NMR ($CDCl_3$) δ (ppm): 0.94 (t, 3H, CH_2CH_2-CH_2CH_3); 1.25 (m, 2H, $CH_2CH_2CH_2CH_3$); 1.32 (m, 2H, CH_2-$CH_2CH_2CH_3$); 3.73 (t, 2H, $CH_2CH_2CH_2CH_3$).

Synthesis of copper sulphide NCs

These syntheses have been performed under a N_2 stream, using a round flask equipped with a Liebig condenser, placed in a heating mantle set at the required temperature. The experimental apparatus was placed inside a fume cupboard equipped with local exhaust ventilation. The thermolysis reactions were performed using as solvents the ionic liquids [THTDP][$N(CN)_2$] and [THTDP][NTf_2]. Two methodologies were employed for the synthesis of copper sulphides; hot-injection of the precursor in ILs and the heating of a batch of the IL containing previously dissolved precursor. A typical synthesis by the injection method was as follows: 0.233 mmol of precursor was dissolved in 4 mL of ILs. This solution was swiftly injected into 16 mL of hot ILs through a syringe, under stirring and N_2 atmosphere. The reaction was kept at the required temperature over 3 h, and then the brown mixture was cooled to 45 °C and methanol was added. The suspended solid was isolated by centrifugation (3461 g over 20 min by using a Hettich EBA 20 centrifuge) and thoroughly washed with methanol. For the batch synthesis, a typical procedure was as follows: 0.233 mmol of precursor was dissolved in 20 mL of ILs under N_2 flow and stirring. The mixture was heated at the required temperature (*e.g.* 180 °C) and kept for 3 h. After cooling the copper sulphide nanopowders were obtained similarly as described above. En route to the synthesis of copper sulphide nanocrystals by the above described methods, and in order to compare the crystalline phase obtained without a solvent, the single-molecule precursors decomposition was also performed in the solid state using a tubular furnace at 500 °C for 2 h, under N_2 atmosphere, placed inside a fume cupboard with efficient exhaust ventilation.

Photocatalytic studies

The photocatalytic activity of as-prepared copper sulphides was preliminary evaluated for the degradation of rhodamine B aqueous solutions under visible-light irradiation, at room temperature. In a typical run, the photocatalyst (10 mg) was dispersed into 150 mL of RhB aqueous solution (20 mg mL^{-1}) by sonication during 15 minutes and stirred for 1 h in the dark, in order to establish adsorption/desorption equilibrium of RhB molecules. The photoreactor was filled with this suspension and then was irradiated by a 400 W halogen lamp (Haloline Eco 400 W, Osram). At regular intervals, aliquots were withdrawn from the reaction mixture and, after centrifugation, the concentration of RhB was estimated by measuring the absorbance and by applying the Beer–Lambert law ($\lambda_{max} = 554$ nm). For comparative purposes, the photocatalytic degradation of RhB was also carried out in the presence of Degussa P25 TiO_2 and H_2O_2 using the same apparatus. Also, in order to clarify the photocatalytic reaction mechanism, the degradation of RhB was performed using a hydroxyl ($^{\bullet}$OH) radical scavenger, *tert*-butanol. The photocatalytic degradation rate was calculated according to the formula:

$$\text{Degradation} = \frac{(1 \quad C_t)}{C_0} \times 100\%$$

where C_0 and C_t are the RhB initial and final concentrations, respectively.

Instrumentation

X-ray power diffraction (XRD) data were collected using a PAN analytical Empyrean X-ray diffractometer equipped with Cu-K_α radiation source ($\lambda = 1.54178$ Å) at 45 kV/40 mA. The UV-Vis

measurement spectra were performed using a Jasco V-560 spectrophotometer. FT-Raman spectra were recorded using a Horiba Jobin-Yvon LabRam HR800 equipped with a multi-channel air cooled (70 °C) CCD (Nd:YAG laser with excitation wavelength of 532 nm, laser power set at 25 mW). X-ray photoelectron spectroscopy (XPS) analysis was performed using a Kratos AXIS Ultra HSA, with VISION software for data acquisition and CASAXPS software for data analysis. The analysis was carried out with a monochromatic Al K_α X-ray source (1486.7 eV), operating at 15 kV (90 W), in fixed analyser transmission mode, with a pass energy of 40 eV for regions ROI and 80 eV for survey. Data acquisition was performed with a pressure lower than 1×10^{-6} Pa, and it was used a charge neutralization system. The effect of the electric charge was corrected by the reference of the carbon peak (284.6 eV). Spectra analysis was performed by peak fitting with Gaussian–Lorentzian peak shape and Shirley type background subtraction (or linear, taking in account the data). Transmission electron microscopy (TEM) was performed using a JEOL JEM-2010 microscope operating at 200 kV. The samples were prepared by placing an aliquot of the ethanolic suspension on a copper grid coated with amorphous carbon film and left to dry in air. Scanning electron microscopy (SEM) analysis was performed using a FEG-SEM Hitachi SU70 microscope, operating at 15 kV, coupled to a Bruker EDX analyzer. The ^{1}H NMR spectra of the precursors in $CDCl_3$ were recorded using a Bruker Avance 300 spectrometer at 300.13 MHz. The chemical shifts were express as δ (ppm) relatively to tetramethylsilane (TMS) as internal reference.

Results and discussion

Phosphonium ILs with two distinct counter anions were used here as solvents (Fig. S1†). As compared to other ILs, these salts show good thermal and chemical stability.[20] This aspect is of particular relevance in this study due to the potential effect of the reaction temperature on the type of polymorph obtained for copper sulphide. Fig. 1 and 2 show the powder XRD patterns for copper sulphide samples obtained by thermal decomposition of the precursor $\{Cu[S_2CN(C_4H_9)_2]_2\}$ in $[TDTHP][N(CN)_2]$ and $[THTDP][NTf_2]$. For comparative purposes, samples prepared by thermolysis of the precursors in oleylamine were also analyzed; oleylamine is a coordinating solvent commonly used in the synthesis of nanocrystals by the hot-injection method.[21]

The XRD identification of copper sulphide phases in polycrystalline samples can be a difficult task due to the diversity of possible phases, similar diffraction patterns and occurrence of mixtures.[22] Indeed, a number of reports have described the synthesis of covellite (CuS) or chalcocite (Cu_2S) but a less number of studies report the formation of non stoichiometric phases ($Cu_{2-x}S$) despite the marked influence of the synthesis conditions on the polymorph obtained. For instance, Fig. 1 shows the diffraction patterns for copper sulphide NCs prepared at 180 °C, by the hot-injection method, using the ILs or oleylamine as solvents. While metastable rhombohedral $Cu_{1.8}S$ (digenite) formed when using $[TDTHP][N(CN)_2]$ and oleylamine, in the presence of $[THTDP][NTf_2]$ the less oxidized phase $Cu_{1.94}S$ (djurleite) was also obtained. This is a first evidence for a solvent effect on the synthesis of copper sulphides polymorphs using the hot-injection method.

As expected, variations in the temperature of synthesis also led to distinct copper sulphide crystalline phases. This is illustrated for the case of using $[TDTHP][N(CN)_2]$ as the solvent, at distinct reaction temperatures, leading to nanocrystalline powders characterized by the powder XRD shown in Fig. 2. Table 1 summarizes the crystalline phases identified for each set of synthesis conditions using the method described here.

There is not an obvious dependency of the phase obtained on the synthesis conditions. Instead, the crystalline phase seems dependent on the conjugation of the type of solvent and reaction temperature that assist the thermolysis of the precursor.

It is instructive to compare the identity of the powders obtained by dry pyrolysis of the precursor $\{Cu[S_2CN(C_4H_9)_2]_2\}$ with

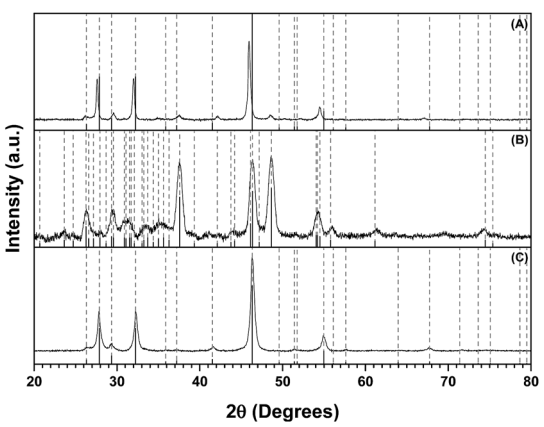

Fig. 1 Powder XRD patterns of copper sulphide NCs prepared by thermolysis of $\{Cu[S_2CN(C_4H_9)_2]_2\}$, at 180 °C, in: (A) $[THTDP][N(CN)_2]$, (B) $[THTDP][NTf_2]$ and (C) oleylamine. The vertical lines correspond to the standard diffractions peaks attributed to copper sulphide: (A) and (C) rhombohedral-digenite type (ICDDPDF file no. 00-047-1748); (B) monoclinic-djurleite type (ICDDPDF file no. 00-023-0959).

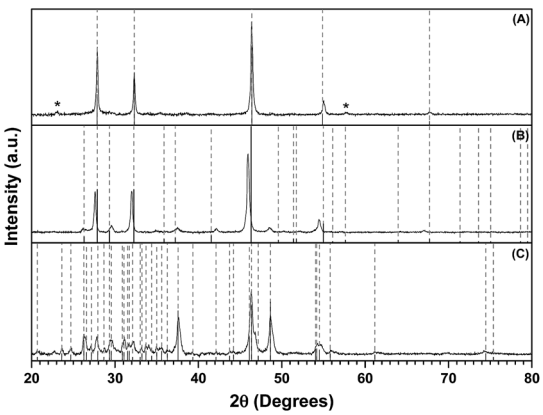

Fig. 2 Powder XRD patterns of copper sulphide samples prepared by thermolysis of $\{Cu[S_2CN(C_4H_9)_2]_2\}$ in $[TDTHP][N(CN)_2]$ at: (A) 120 °C, (B) 180 °C and (C) 240 °C. The vertical lines correspond to the standard diffractions peaks attributed to copper sulphide: (A) cubic phase-digenite type (ICDDPDF file no. 00-024-0061), (B) rhombohedral phase-digenite type (ICDDPDF file no. 00-047-1748) and (C) monoclinic phase with djurleite type (ICDDPDF file no. 00-023-0959).

Table 1 Copper sulphide nanophases obtained at different reaction conditions

Solvent	Temp (°C)	Average size[a] (nm)	Phase	JCPDS file no.
[THTDP][$N(CN)_2$]	120	43	$Cu_{1.8}S$ cubic	00 024 0061
	180	30	$Cu_{1.8}S$ rhombohedral	00 047 1748
	240	22	$Cu_{1.94}S$ monoclinic	00 023 0959
[THTDP][NTf_2]	120			
	180	11	$Cu_{1.94}S$ monoclinic	00 023 0959
	240	42	$Cu_{1.8}S$ rhombohedral	00 047 1748
Oleylamine	120	41	$Cu_{1.8}S$ rhombohedral	00 047 1748
	180	18	$Cu_{1.8}S$ rhombohedral	00 047 1748
	240	16	CuS hexagonal	00 006 0464

[a] Calculated from XRD using the Debye Scherrer formula.

that one produced by the corresponding process of liquid phase thermolysis. The solid state pyrolysis of such precursor led to the formation of cubic copper sulphide-digenite structure (Fig. S2†), which similarly to most of the liquid phase thermolysis products (Table 1) also resulted from a partial reduction of Cu(II) ions, in the complex, to Cu(I) ions in the final metal sulphide. However, a distinct phase was obtained in this case, thus suggesting that there is an influence of the solvent on the type of crystalline phase obtained. Previously, Sceney *et al.*[23] have reported the chalcocite phase (Cu_2S) as the product from the thermal decomposition of $\{Cu[S_2CN(C_2H_5)_2]_2\}$, with concomitant reduction of Cu(II) to Cu(I). Here, the copper sulphide obtained from dry pyrolysis corresponds to $Cu_{1.8}S$,[22] thus our results are in line with other reports,[2] in the sense that the most reduced form Cu_2S (chalcocite) was not observed for any of the samples obtained by the thermolysis of the Cu(II) dithiocarbamate precursor. Fig. 3 shows *in situ* XRD patterns for a rhombohedral digenite sample submitted to variable temperature treatment (30–400 °C).

The structural changes associated to the temperature dependent XRD patterns can be divided in two main stages: (i) up to 280 °C, there were no significant changes in the crystalline phase; (ii) above this temperature, up to 400 °C, the diffraction peaks are in agreement with the presence of $Cu_{1.94}S$.

In order to clarify the valence of Cu and S in the several copper sulfide nanocrystals prepared, XPS analysis was performed by using the C 1s peak as reference. The XPS survey spectra indicate the presence of Cu and S as well as C and O adsorbed due to exposure to air (Fig. S3†). The XPS spectra of the Cu 2p and S 2p core levels for the rhombohedral (digenite type) and covellite samples are shown in Fig. 4. The Cu 2p core level XPS spectra for the three types of copper sulphide show the binding energies corresponding to Cu $2p_{3/2}$ and $2p_{1/2}$. The Cu $2p_{3/2}$ spectrum of covellite nanocrystals shows two peaks at 932.4 eV and 933.6 eV, which are in agreement with published values for Cu^+ and Cu^{2+}.[24b,27] For digenite ($Cu_{1.8}S$) two peaks are observed, at 932.2 eV and 933.3 eV, showing the presence of Cu^+ and Cu^{2+} sites. The Cu $2p_{3/2}$ region of covellite was characterized by an asymmetric tail, which has been reported for this crystalline phase.[28] The asymmetric shape of the peaks were

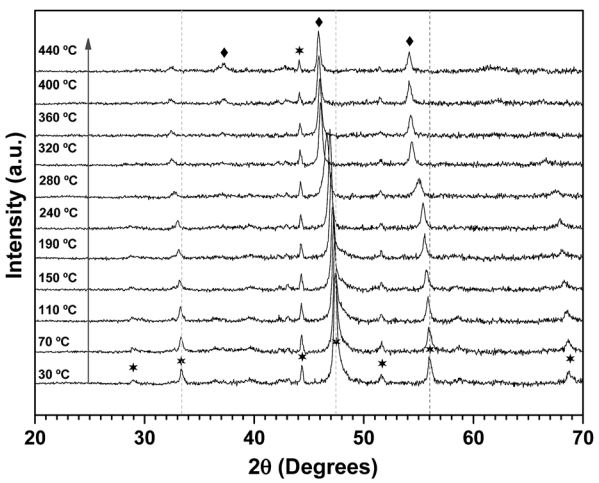

Fig. 3 *In situ* powder XRD patterns for nanocrystalline copper sulphide submitted to thermal treatment: ★ rhombohedral $Cu_{1.8}S$; ◆ monoclinic $Cu_{1.94}S$.

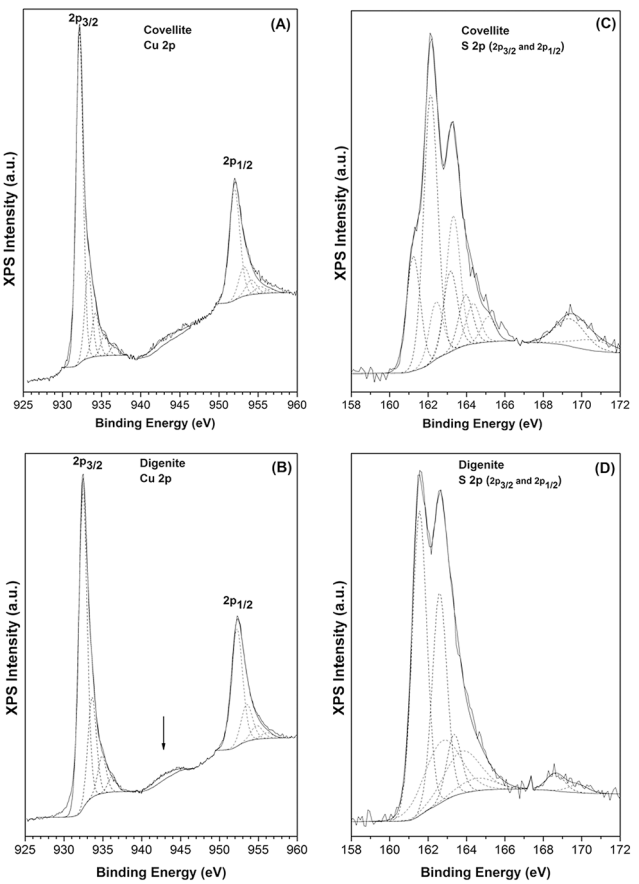

Fig. 4 Fitted XPS spectra of copper sulphide (Cu 2p, S 2p) phases: CuS (A and C) and $Cu_{1.8}S$ (B and D).

slightly reduced from covellite to digenite nanocrystals. In addition, for both structures, a weak peak corresponding to a satellite (indicated by an arrow) was observed around 943 eV, indicating the paramagnetic chemical state of Cu^{2+}.[27a]

The S 2p XPS core level for covellite is characterized by three peak profiles typical of covellite.[29] Peak fitting indicates that there are distinct sulphur sites in the sample. The peaks at 161.2 and 162.1 eV correspond to the S $2p_{3/2}$ core levels for S^{2-} and S_2^{2-}, respectively. In the case of digenite, the peaks corresponding to sulphides and disulphide are also observed and appear at 161.6 eV and 162.6 eV, respectively. The peaks at 168.6 eV and 169.4 eV, in S 2p core level XPS spectrum for digenite and covellite, respectively, are attributed to sulphate due to adventitious surface oxidation.[27c,30c]

Depending on the stoichiometry, copper sulphide ($Cu_{2-x}S$) materials show different values for the energy band gap (E_g) and this is has been of great interest for a number of photo-applications.[2,17c,24] The energy band gap varies from 1.3 eV in djurleite ($x = 0.06$), 1.75 eV in digenite ($x = 0.2$) and 2.2 eV in covellite ($x = 1$).[25] Additionally, band gap tuning can also be accessed by varying particle size of the semiconductor (quantum size effects) leading to new possibilities for the application of these materials. Table 1 shows the crystallite size for the several copper sulphides prepared in this work, as determined by the Debye–Scherrer equation.[26] Although these values give a crude estimate on particle size, overall the observed crystallite size ranges between 11 and 43 nm. These dimensions are above 10 nm, which has been reported as the size threshold above which quantum size effects are expected to occur for this material.[2] However, this assumption needs further confirmation because the dielectric constants for $Cu_{2-x}S$ materials also change with chemical composition that might lead into larger exciton Bohr radius.[2] For clarifying this point the experimental visible spectra of the $Cu_{2-x}S$ samples are of great utility in the current study. For example, Fig. 5 indicates that the optical band gap for samples prepared in the IL $[TDTHP][N(CN)_2]$ is close to the values for the respective E_g of the bulk materials. Thus the optical band gap of covellite (CuS) and rhombohedral digenite nanocrystalline samples as prepared by liquid phase thermolysis is 2.2 eV and 1.7 eV, respectively. This indicates that the E_g in both cases are basically consistent with that of bulk CuS (2.2 eV) and bulk $Cu_{1.8}S$ (1.75 eV). Also for the djurleite sample, the optical data in Fig. 5 gives a band gap of 1.4 eV of the bulk sample, which is also in agreement with relatively large particles, as illustrated for this case in Fig. 6.

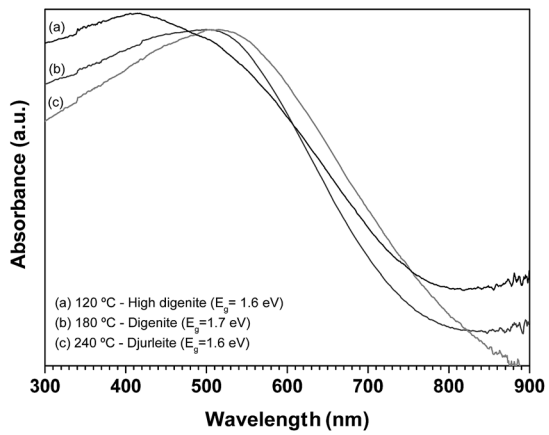

Fig. 5 UV-Vis absorption spectra of nanocrystalline copper sulphide samples prepared in $[TDTHP][N(CN)_2]$ at: (a) 120 °C, (b) 180 °C and (c) 240 °C.

Studies of copper sulphide NCs as heterogeneous photocatalysts for the degradation of organic dyes are seldom reported. Recently, Ding *et al.*[31] have reported the photocatalytic properties of CuS nanoflowers using rhodamine B and, after 2 hours under halogen lamp irradiation, a degradation rate close to 90% was found. Other studies have shown that self-assembled structures and nanodisks of CuS can degrade 85% and 93% of RhB, respectively, over 2 h under visible-light irradiation.[32] Li *et al.* have described the photocatalytic activity of CuS structures for the decomposition of methylene blue under solar light irradiation.[1f,32] Nanocrystals of CuS were also evaluated on the photodegradation of RhB under visible light irradiation, showing that less than 20% of RhB is degraded. In this study, the authors have shown that the photodegradation efficiency of the CuS could be enhanced by its encapsulation with ZnS shells, achieving ~50% degradation after irradiation by visible light during 2 h.[1h] More recently, various types of copper sulphide have been used in the photodegradation of rhodamine B; in this case the presence of H_2O_2 as co-catalyst improved the

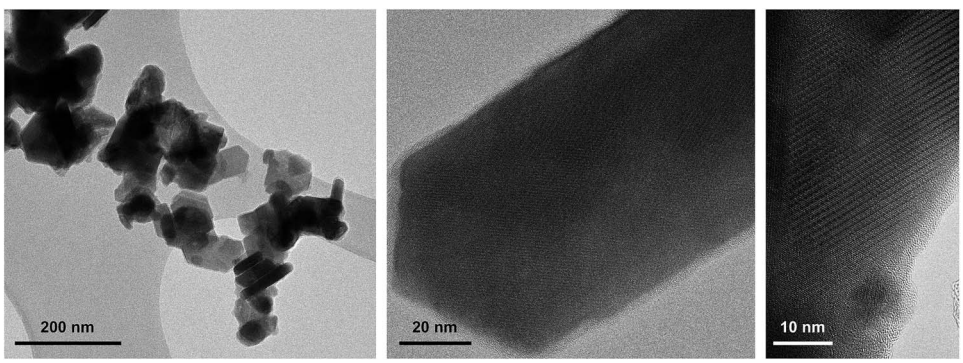

Fig. 6 TEM images of djurleite nanocrystals obtained in $[TDTHP][N(CN)_2]$ ionic liquid at 240 °C (injection temperature).

photodegradation rate to 98%, at room temperature.[1g] Also, other organic pollutants such as nitrobenzene and 4-nitrophenol have been efficiently degraded under visible light irradiation by using CuS photocatalysts.[33] An important feature for the nanomaterials obtained by the ionic liquid route as described here is their easy dispersion in water, hence resulting in colloidal stable suspensions. Together with the possibility of crystalline phase and optical band gap tuning, these materials can be of great interest for heterogeneous semiconductor photocatalysis. In order to perform a preliminary assessment of their potential in visible photocatalysis, selected copper sulphides nanophases were tested in the presence of H_2O_2. In these tests, RhB was selected as an organic dye model because it shows strong absorption in the visible region (554 nm) and is photostable in the absence of photocatalyst. In fact, negligible values of RhB degradation under visible-light irradiation were observed in the absence of catalyst.

Fig. 7(I) shows the percentage of photodegradation of RhB as function of time of light irradiation in the presence and absence of $Cu_{1.8}S$, at different reaction conditions. It is clear that the photodegradation of RhB in the presence of either $Cu_{1.8}S$ or H_2O_2 alone was very low; about 10% and 3.5% of RhB were degraded after 120 minutes, respectively (Fig. 7c and d). Furthermore, in presence of both $Cu_{1.8}S$ and H_2O_2 but in dark conditions, only 25% of RhB was decomposed after 2 h irradiation. Still, for the conditions investigated, the maximum RhB photodegradation (close to 100%) after 2 h irradiation, was observed in presence of djurleite and by adding to the system 1.5 mL of H_2O_2 (30% w/w). Fig. 7(II) compares the photodegradation rate of RhB, as a function of time, in presence of three copper sulphide NCs prepared by the IL route: rhombohedral digenite, djurleite and covellite. Both djurleite and digenite nanophases show high visible-light photocatalytic activity, with fast RhB degradation rate at the early stage of the photocatalytic process, with about 80% of RhB degraded after 15 minutes. On the other hand, covellite exhibited weaker photocatalytic activity than djurleite and digenite, *circa* 22% degradation after 120 minutes light irradiation. In fact, both digenite and djurleite polytypes exhibit strong absorption in the visible region, while covellite absorbs strongly in the near-IR region (Fig. S4†). For sake of comparison, the photocatalytic activity of commercial Degussa P25 TiO_2 was also evaluated in these conditions. The photodegradation of RhB after 15 min and 120 min was 12% and 84%, respectively, which are values lower than those achieved in the presence of djurleite and digenite, under visible light irradiation; it is well known that P25 TiO_2 performs more efficiently under UV irraditation.[34]

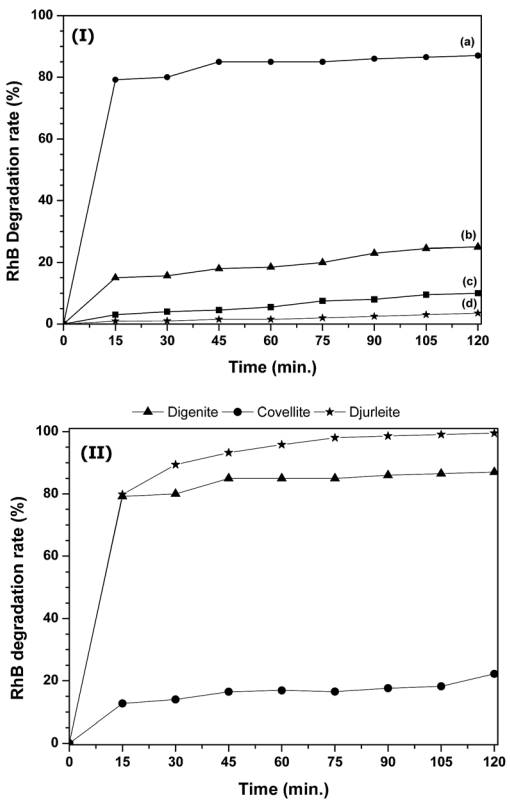

Fig. 7 Percentage rate for the degradation of RhB aqueous solutions (20 mg L^{-1}). (I) $Cu_{1.8}S$ as photocatalyst: (a) H_2O_2 30% (w/w); 400 W halogen lamp irradiation; (b) H_2O_2 30% (w/w); dark conditions; (c) no co-catalyst; 400 W halogen lamp irradiation; (d) no catalyst, H_2O_2 30% (w/w); 400 W halogen lamp irradiation. (II) Comparison of the photocatalytic activity of $Cu_{1.8}S$, $Cu_{1.94}S$ and CuS nanomaterials, assisted by H_2O_2 30% (w/w) as co-catalyst and under 400 W halogen lamp irradiation. Lines aim to guide the eye.

In the presence of djurleite, for which maximum RhB photodegradation was achieved, the wavelength for maximum absorption (λ_{max}) of the dye was slightly shifted from 554 nm to 530 nm, along with a decrease in the absorbance during the photocatalytic reaction. A similar blue shift was reported for the RhB oxidation using metal oxides as photocatalysts, which was associated to stepwise removal of the *N*-ethyl group in the degradation of RhB (*N*,*N*,*N*′,*N*′-tetra-ethylated rhodamine).[35]

The characteristic λ_{max} for RhB and for the de-ethylated rhodamine species are 554 nm (RhB), 535 nm (*N*,*N*,*N*′-triethylated rhodamine), 522 nm (*N*,*N*-di-ethylated rhodamine) and 498 nm (rhodamine), respectively.[36] Thus, these results suggest that the RhB photodegradation occurs *via* de-ethylation of a single *N*-ethyl group followed then by oxidation of the dye.

Several research groups have investigated the photocatalytic mechanism applied to the degradation of water dissolved organic dyes, using copper sulfide as the catalyst.[32,33,37,44] Based on the literature, it is possible to suggest a mechanism that also takes into account our own data. Hence, when energy superior to the E_g of copper sulfide irradiates the semiconductor, photogenerated electrons (e^-) and holes (h^+) are formed, respectively in the conduction band (CB) and valence band (VB). The photogenerated charge carriers (e^- and h^+) have the ability to promote chemical processes with adsorbed dye molecules at the particles' surfaces, though electron–hole recombination is a competitive process.[38] Photogenerated electrons will be trapped by dissolved O_2, generating superoxide radicals ($O_2^{-\bullet}$), which can further combine with holes to yield $^{\bullet}OH$ radicals. Photogenerated electrons can also be captured by H_2O_2, which is an electron acceptor, increasing the amount of reactive hydroxyl radicals ($^{\bullet}OH$) and limiting electron–hole recombination. The hydroxyl radicals can also to be obtained by the

interaction of –OH and photogenerated holes. In fact, when the photodegradation of RhB with H_2O_2 was performed in the presence of *tert*-butanol, a hydroxyl ($^{\bullet}OH$) radical scavenger, significant decrease on the RhB degradation was observed, suggesting that RhB degradation proceed mainly *via* radical mechanism. However, chemical generated hydroxyl radicals due to the hemolytic cleavage of H_2O_2 (Fenton-type reaction) have also been considered to be involved in the photocatalytic behavior of CuS, which can thus explain its catalytic activity in dark conditions.[43,44]

Conclusions

Copper sulphide nanocrystals were synthesized using the decomposition of Cu(II) alkyldithiocarbamate complexes in ILs. This method yields water dispersible nanocrystals of diverse $Cu_{2-x}S$ polytypes, which were further exploited as heterogeneous photocatalysts on RhB degradation under visible-light irradiation, in presence of H_2O_2 as co-catalyst. Preliminary assessment of the copper sulphide nanophases obtained by this IL route, shows that the degradation rate of RhB seem to depend on the type of copper sulphide obtained and their ability to disperse in water. So, the best degradation values of RhB were obtained in the presence of djurleite and digenite, both prepared in ILs, showing almost 100% of degradation after 120 minutes. The copper sulphide obtained in oleylamine are less dispersed in water, giving the lowest values of RhB degradation. Therefore, the possibility to obtain a particular polymorph in controlled synthesis conditions is of great relevance due to distinct photocatalytic behavior. Future work on these systems will attempt to investigate the reuse of these catalysts namely as supported materials.

Acknowledgements

This research was financed in the scope of the FCT Project UTAP-ICDT/CTMNAN/0025/2014 and through the project CICECO-Aveiro Institute of Materials, POCI-01-0145-FEDER-007679 (FCT Ref. UID/CTM/50011/2013), financed by national funds through the FCT/MEC and when appropriate co-financed by FEDER under the PT2020 Partnership Agreement. The authors are very grateful to Dr Carlos Sá (CEMUP), Dr Marta Ferro and MSc M. C. Azevedo for technical support. A. C. E. also thanks FCT for a post-doctoral grant (SFRH/BPD/86780/2012).

Notes and references

1 (*a*) Q. Tian, M. Tang, Y. Sun, R. Zou, Z. Chen, M. Zhu, S. Yang, J. Wang, J. Wang and J. Hu, *Adv. Mater.*, 2011, **23**, 3542–3547; (*b*) M. Zhou, R. Zhang, M. Huang, W. Lu and S. Song, *J. Am. Chem. Soc.*, 2010, **132**, 15351; (*c*) X. Zhang, G. Wang, A. Gu, Y. Wei and B. Fang, *Chem. Commun.*, 2008, 5945–5947; (*d*) A. Qurashi, *Metal Chalcogenide Nanostructures for Renewable Energy Applications*, Wiley, New Jersey, 2014; (*e*) A. Mills and S. Le Hunte, *J. Photochem. Photobiol., A*, 1997, **108**, 1–35; (*f*) F. Li, J. Wu, Q. Qin, Z. Li and X. Huang, *Powder Technol.*, 2010, **198**, 267–274; (*g*) M. Wang, F. Xie, W. Li, M. Chen and Y. Zhao, *J. Mater. Chem. A*, 2013, **1**, 8616–8621; (*h*) U. T. D. Thuy, N. Q. Liem, C. M. Parlett, G. M. Lalev and K. Wilson, *Catal. Commun.*, 2014, **44**, 62–67; (*i*) S. J. Oh, N. E. Berry, J.-H. Choi, E. A. Gaulding, T. Paik, S.-H. Hong, C. B. Murray and C. R. Kagan, *ACS Nano*, 2013, **7**, 2413–2421.

2 Y. Zhao, H. Pan, Y. Lou, X. Qiu, J. Zhu and C. Burda, *J. Am. Chem. Soc.*, 2009, **131**, 4253–4261.

3 (*a*) C. Tan, Y. Zhu, R. Lu, P. Xue, C. Bao, X. Liu, Z. Fei and Y. Zhao, *Mater. Chem. Phys.*, 2005, **91**, 44–47; (*b*) A. Baray-Calderón, R. Galindo, J. L. Maldonado, O. Martínez-Alvarez, L. S. Acosta-Torres, J. Santos-Cruz, J. de la Fuente-Hernández and M. C. Arenas-Arrocena, *MRS Online Proc. Libr.*, 2015, 1748.

4 (*a*) X. Yan, E. Michael, S. Komarneni, J. R. Brownson and Z.-F. Yan, *Ceram. Int.*, 2013, **39**, 4757–4763; (*b*) Y. Wang, X. Ai, D. Miller, P. Rice, T. Topuria, L. Krupp, A. Kellocka and Q. Song, *CrystEngComm*, 2012, **14**, 7560–7562; (*c*) T. Thongtem, A. Phuruangrat and S. Thongtem, *Mater. Lett.*, 2010, **64**, 136–139.

5 (*a*) P. Bera and I. L. Seok, *Solid State Sci.*, 2012, **14**, 1126–1132; (*b*) Y. Li, L. Zhang, J. C. Yu and S.-H. Yu, *Progress in Natural Science: Materials International*, 2012, **22**, 585–591; (*c*) M. Lot, T. Machani, D. P. Rossi and K. E. Plass, *Chem. Mater.*, 2011, **23**, 3032–3038; (*d*) J. Liu and D. Xue, *Mater. Res. Bull.*, 2010, **45**, 309–313; (*e*) C. An, S. Wang, J. He and Z. Wang, *J. Cryst. Growth*, 2008, **310**, 266–269; (*f*) X. P. Shen, H. Zhao, H. Q. Shu, H. Zhou and A. H. Yuan, *J. Phys. Chem. Solids*, 2009, **70**, 422–424.

6 I. P. Parkin, *Chem. Soc. Rev.*, 1996, **25**, 199–207.

7 (*a*) M. Kristl, N. Hojnik, S. Gyergyek and M. Drofenik, *Mater. Res. Bull.*, 2013, **48**, 1184–1188; (*b*) H. Wang, J. R. Zhang, X. N. Zha, S. Xu and J. J. Zhu, *Mater. Lett.*, 2002, **55**, 253–258; (*c*) R. V. Kumar, O. Palchik, Y. Koltypin, Y. Diamant and A. Gedanken, *Ultrason. Sonochem.*, 2002, **9**, 65–70.

8 (*a*) J. N. Solanki, R. Sengupta and Z. V. P. Murthy, *Solid State Sci.*, 2010, **12**, 1560–1566; (*b*) L. Chen, Y. Shang, H. Liu and Y. Hu, *Mater. Des.*, 2010, **31**, 1661–1665; (*c*) I. Lisiecki, F. Billoudet and M. P. Pileni, *J. Mol. Liq.*, 1997, **72**, 251–261.

9 C. M. Simonescu, V. E. Teodorescu and C. Căpăþînă, *Rev. Chim.*, 2008, **59**, 1327–1329.

10 V. Bansal and S. K. Bhargava, in *Ionic Liquids: Theory, Properties, New Approaches*, ed. A. Kokorin, Intech, Rijeka, 2011, ch. 16, pp. 367–382.

11 K. Yao, W. Lu and J. Wang, *Mater. Chem. Phys.*, 2011, **130**, 1175–1181.

12 H. Kalviri and F. M. Kerton, *Green Chem.*, 2011, **13**, 681–686.

13 (*a*) Ş. Neaţu, J. A. Maciá-Agulló and H. Garcia, *Int. J. Mol. Sci.*, 2014, **15**, 5246–5262; (*b*) S. N. Habisreutinger, L. Schmidt-Mende and J. K. Stolarczyk, *Angew. Chem., Int. Ed.*, 2013, **52**, 7372–7408.

14 (*a*) A. Sobczyński and A. Dobosz, *Pol. J. Environ. Stud.*, 2001, **10**, 195–205; (*b*) C. Chen, W. Ma and J. Zhao, *Chem. Soc. Rev.*, 2010, **39**, 4206–4219.

15 (*a*) R. Vogel, P. Hoyer and H. Weller, *J. Phys. Chem.*, 1994, **98**, 3183–3188; (*b*) D. Robert, *Catal. Today*, 2007, **122**, 20–26; (*c*) J. C. Kim, J. Choi, Y. B. Lee, J. H. Hong, J. I. Lee, J. W. Yang,

W. I. Lee and N. H. Hur, *Chem. Commun.*, 2006, 5024–5026; (*d*) Y. Bessekhouad, D. Robert and J. V. Weber, *J. Photochem. Photobiol., A*, 2004, **163**, 569–580.

16 R. Nagarajan and T. A. Hatton, *Nanoparticles: Synthesis, Stabilization, Passivation and Functionalization*, American Chemical Society, Washington, 2008.

17 (*a*) S. V. Bagul, S. D. Chavhan and R. Sharma, *J. Phys. Chem. Solids*, 2007, **68**, 1623–1629; (*b*) S. H. Jiao, L. F. Xu, K. Jiang and D. S. Xu, *Adv. Mater.*, 2006, **18**, 1174–1177; (*c*) M. T. S. Nair, L. Guerrero and P. K. Nair, *Semicond. Sci. Technol.*, 1998, **13**, 1164–1169.

18 S. C. Ngo, K. K. Banger, M. J. DelaRosa, P. J. Toscano and J. T. Welch, *Polyhedron*, 2003, **22**, 1575–1583.

19 T. Trindade, O. C. Monteiro, P. O'Brien and M. Motevalli, *Polyhedron*, 1999, **18**, 1171–1175.

20 C. J. Bradaric, A. Downard, C. Kennedy, A. J. Robertson and Y. Zhou, *Green Chem.*, 2003, **5**, 143–152.

21 S. Mourdikoudis and L. M. Liz-Marzán, *Chem. Mater.*, 2013, **25**, 1465–1476.

22 D. J. Chakrabarti and D. E. Laughlin, *Bull. Alloy Phase Diagrams*, 1983, **4**, 254–271.

23 C. G. Sceney, J. F. Smith, J. O. Hill and R. J. Magee, *J. Therm. Anal.*, 1976, **9**, 415–423.

24 (*a*) L. Reijnen, B. Meester, A. Goossens and J. Schoonman, *Mater. Sci. Eng., C*, 2002, **19**, 311–314; (*b*) S. Li, H. Z. Wang, W. W. Xu, H. L. Si, X. J. Tao, S. Lou, Z. Du and L. S. Li, *J. Colloid Interface Sci.*, 2009, **330**, 483–487; (*c*) Y. Wu, C. Wadia, W. Ma, B. Sadtler and A. P. Alivisatos, *Nano Lett.*, 2008, **8**, 2551–2555.

25 O. Madelung, *Semiconductor, Other than Group IV Elements and III–V Compounds*, Springer, Berlin, 1992.

26 B. D. Cullity, *Elements of X-ray Diffraction*, Addison-Wesley, Reading, MA, 1956.

27 (*a*) J. F. Moulder, W. F. Stickle, P. E. Sobol and K. D. Bomben, *Handbook of X-Ray Photoelectron Spectroscopy*, Physical Electronics Division, USA, 1995; (*b*) X. Li, H. Shen, J. Niu, S. Li, Y. Zhang, H. Wang and L. S. Li, *J. Am. Chem. Soc.*, 2010, **132**, 12778–12779; (*c*) V. Krylova and M. Andrulevičius, *Int. J. Photoenergy*, 2009, **2009**, 1–8; (*d*) M. Kundu, T. Hasegawa, K. Terabe, K. Yamamoto and M. Aono, *Sci. Technol. Adv. Mater.*, 2008, **9**, 035011; (*e*) Y. C. Zhang, T. Qiao and X. Ya, *J. Cryst. Growth*, 2004, **268**, 64–70; (*f*) E. Kurmaev, J. Van Ek, D. Ederer, L. Zhou, T. Callcott, R. Perera, V. Cherkashenko, S. Shamin, V. Trofimova and S. Bartkowski, *J. Phys.: Condens. Matter*, 1998, **10**, 1687–1691; (*g*) M. C. Biesinger, L. W. M. Lau, A. R. Gerson and R. S. C. Smart, *Appl. Surf. Sci.*, 2010, **257**, 887–898; (*h*) J. Yu, J. Zhang and S. Liu, *J. Phys. Chem. C*, 2010, **114**, 13642–13649.

28 S. W. Goh, A. N. Buckley, R. N. Lamb, R. A. Rosenberg and D. Moran, *Geochim. Cosmochim. Acta*, 2006, **70**, 2210–2228.

29 Y. Xie, A. Riedinger, M. Prato, A. Casu, A. Genovese, P. Guardia, S. Sottini, C. Sangregorio, K. Miszta, S. Ghosh, T. Pellegrino and L. Manna, *J. Am. Chem. Soc.*, 2013, **135**, 17630–17637.

30 (*a*) H. T. Zhu, J. X. Wang and G. Y. Xu, *Cryst. Growth Des.*, 2009, **9**, 633–638; (*b*) M. Yin, C. K. Wu, Y. B. Lou, C. Burda, J. T. Koberstein, Y. M. Zhu and S. O'Brien, *J. Am. Chem. Soc.*, 2005, **127**, 9506–9511; (*c*) D. P. Griffis and R. W. Linton, *Surf. Interface Anal.*, 1982, **4**, 197–203.

31 T. Y. Ding, M. S. Wang, S. P. Guo, G. C. Guo and J. J. Huang, *Mater. Lett.*, 2008, **62**, 4529–4531.

32 Y.-Q. Zhang, B.-P. Zhang and L.-F. Zhu, *RSC Adv.*, 2014, **4**, 59185–59193.

33 M. Saranya, R. Ramachandran, E. J. J. Samuel, S. K. Jeong and A. N. Grace, *Powder Technol.*, 2015, **279**, 209–220.

34 G. Xiao, X. Huang, X. Liao and B. Shi, *J. Phys. Chem. C*, 2013, **117**, 9739–9746; H. Zhang, X. Lv, Y. Li, Y. Wang and J. Li, *ACS Nano*, 2010, **4**, 380–386; M. Božič, V. Vivod, R. Vogrinčič, I. Ban, G. Jakša, S. Hribernik, D. Fakin and V. Kokol, *J. Colloid Interface Sci.*, 2016, **465**, 93–105.

35 (*a*) S. Hu, J. Zhu, L. Wu, X. Wang, P. Liu, Y. Zhang and Z. Li, *J. Phys. Chem. C*, 2011, **115**, 460–467; (*b*) L. Pan, J. Zou, X. Zhang and L. Wang, *J. Am. Chem. Soc.*, 2011, **133**, 10000–10002.

36 T. Wu, G. Liu, J. Zhao, H. Hidaka and N. Serpone, *J. Phys. Chem. B*, 1998, **102**, 5845–5851.

37 L. Cai, Y. Sun, W. Li, W. Zhang, X. Liu, D. Ding and N. Xu, *RSC Adv.*, 2015, **5**, 98136–98143.

38 M. R. Hoffmann, S. T. Martin, W. Y. Choi and D. W. Bahnemannt, *Chem. Rev.*, 1995, **95**, 69–96.

39 (*a*) W. L. Zhang, Y. G. Sun, Z. Y. Xiao, W. Y. Li, B. Li, X. J. Huang, X. J. Liu and J. Q. Hu, *J. Mater. Chem. A*, 2015, **3**, 7304–7313; (*b*) S. Sun, D. Deng, C. Kong, X. Song and Z. Yang, *Dalton Trans.*, 2012, **41**, 3214–3222.

40 Y. Wang, L. Zhang, H. Jiu, N. Li and Y. Sun, *Appl. Surf. Sci.*, 2014, **303**, 54–60.

41 M. Saranya, R. Ramachandran, P. Kollu, S. K. Jeong and A. N. Grace, *RSC Adv.*, 2015, **5**, 15831–15840.

42 J. Zhang, J. Yu, Y. Zhang, Q. Li and J. R. Gong, *Nano Lett.*, 2011, **11**, 4774–4779.

43 S. H. Bossmann, E. Oliveros, S. Göb, S. Siegwart, E. P. Dahlen, L. Payawan, M. Straub, M. Wörner and A. M. Braun, *J. Phys. Chem. A*, 1998, **102**, 5542–5550.

44 W. Xu, S. Zhu, Y. Liang, Z. Li, Z. Cui, X. Yang and A. Inoue, *Sci. Rep.*, 2015, **5**, 18125.

